Radiometric Modeling of Cavernous Targets to Assist in the Determination of Absolute Temperature for Input to Process Models

Matthew Montanaro[a], Carl Salvaggio[a], Scott D. Brown[a], David W. Messinger[a], Adam A. Goodenough[a], Alfred J. Garrett[b] and Eliel Villa-Aleman[b]

[a]Rochester Institute of Technology, 54 Lomb Memorial Drive, Rochester, NY, USA;
[b]Savannah River National Laboratory, Building 735-A, Office B108, Aiken, SC, USA

ABSTRACT

Determining the temperature of an internal surface within cavernous targets, such as the interior wall of a mechanical draft cooling tower, from remotely sensed imagery is important for many surveillance applications that provide input to process models. The surface leaving radiance from an observed target is a combination of the self-emitted radiance and the reflected background radiance. The self-emitted radiance component is a function of the temperature-dependent blackbody radiation and the view-dependent directional emissivity. The reflected background radiance component depends on the bidirectional reflectance distribution function (BRDF) of the surface, the incident radiance from surrounding sources, and the BRDF for each of these background sources. Inside a cavity, the background radiance emanating from any of the multiple internal surfaces will be a combination of the self-emitted and reflected energy from the other internal surfaces as well as the downwelling sky radiance. This scenario provides for a complex radiometric inversion problem in order to arrive at the absolute temperature of any of these internal surfaces. The cavernous target has often been assumed to be a blackbody, but in field experiments it has been determined that this assumption does not always provide an accurate surface temperature. The Digital Imaging and Remote Sensing Image Generation (DIRSIG) modeling tool is being used to represent a cavity target. The model demonstrates the dependence of the radiance reaching the sensor on the emissivity of the internal surfaces and the multiple internal interactions between all the surfaces that make up the overall target. The cavity model is extended to a detailed model of a mechanical draft cooling tower. The predictions of derived temperature from this model are compared to those derived from actual infrared imagery collected with a helicopter-based broadband infrared imaging system collected over an operating tower located at the Savannah River National Laboratory site.

Keywords: CAVERNOUS TARGETS, THERMAL IMAGERY, ABSOLUTE TEMPERATURE, APPARENT TEMPERATURE, APPARENT EMISSIVITY, BRDF, SYNTHETIC IMAGE GENERATION

1. INTRODUCTION

The temperature of a target may be estimated from remotely sensed thermal infrared imager provided information about the emissivity is known. Differences between the apparent temperature determined for an object from observed thermal data may result from either differences from the assumed optical properties, such as emissivity and reflectance, or from differences in the bulk properties and temperature, or from the geometry of the object [1]. The radiance from a target of interest is a composite of the self-emission of the target surface and the reflected radiance from background sources. For an exposed, level surface the reflected background is the reflected downwelled radiance from the skydome. For a cavernous object, the background radiance is a collection of the self-emitted and reflected energies from the interior surfaces of the cavity as well as the downwelling sky radiance. The apparent temperature of the cavity is therefore dependent on the optical and bulk properties of the cavity surfaces and on the internal geometry of the cavity. The DIRSIG software was used to model a cavity to study such effects. DIRSIG is a first principles physics-based synthetic image generation application developed by the Digital Imaging and Remote Sensing (DIRS) Laboratory at the Rochester Institute of Technology (RIT) [2]. A study was performed to determine the effect of the number of internal reflections and of the properties of the internal surfaces on the derived temperature of the cavity and those results are presented here.

Send correspondence to Matthew Montanaro: E-mail: mxm9876@cis.rit.edu, Telephone: 1 585 475 6380

Algorithms and Technologies for Multispectral, Hyperspectral, and Ultraspectral Imagery XIII, edited by Sylvia S. Shen, Paul E. Lewis, Proc. of SPIE Vol. 6565
656511, (2007) · 0277-786X/07/$18 · doi: 10.1117/12.718666

2. BACKGROUND

All materials both emit and reflect radiant energy. The emitted energy is a result of the temperature of the object. The reflected energy is the result of radiant energy from background sources scattering off the object. Both sources of energy must be taken into account when extracting the apparent temperature of a target.

2.1. Self-Emitted Radiance

Self emission from a blackbody is dependent on the temperature of the object and is defined through Planck's equation as,

$$L_{BB}(\lambda, T) = \frac{2hc^2}{\lambda^5}\left[e^{\frac{hc}{\lambda kT}} - 1\right]^{-1} \qquad \left[\frac{W}{m^2\, sr\, \mu m}\right], \tag{1}$$

where h is Planck's constant, c is the speed of light in vacuum, k is Boltzmann's constant, T is the temperature of the object, and λ is the wavelength. Real-world objects are not perfect emitters and will therefore emit less radiance than a blackbody. The spectral emissivity, $\epsilon(\lambda)$, is a measure of the effectiveness of an object as a radiator. For Lambertian surfaces, the radiance is distributed equally into the hemisphere above the surface [1]. The self-emission for Lambertian surfaces is defined as,

$$L(\lambda, T) = \epsilon(\lambda) L_{BB}(\lambda, T) \qquad \left[\frac{W}{m^2\, sr\, \mu m}\right]. \tag{2}$$

Most materials are not Lambertian and will radiate more in some directions than in others. The emissivity term is modified to incorporate this dependence on view angle. The self-emission for non-Lambertian surfaces is then,

$$L(\theta, \phi, \lambda, T) = \epsilon(\theta, \phi, \lambda) L_{BB}(\lambda, T) \qquad \left[\frac{W}{m^2\, sr\, \mu m}\right]. \tag{3}$$

The term $\epsilon(\theta, \phi, \lambda)$ is known as the directional emissivity.

2.2. Reflected Radiance

The reflective analog of directional emissivity is the bidirectional reflectance distribution function (BRDF). It is defined as the ratio of the radiance, L, reflected from the surface into the direction (θ_r, ϕ_r) to the irradiance, E, incident on the surface from direction (θ_i, ϕ_i) [3]. The unpolarized BRDF is stated mathematically as,

$$\rho(\theta_i, \phi_i, \theta_r, \phi_r, \lambda) = \frac{L(\theta_r, \phi_r, \lambda)}{E(\theta_i, \phi_i, \lambda)} \qquad \left[sr^{-1}\right]. \tag{4}$$

The BRDF describes the distribution of reflected radiance into the hemisphere from a given source geometry. It can be thought of as a probability distribution function for the reflected radiance in any direction [3]. Figure (1) illustrates various BRDF shapes for different materials.

The integral of the BRDF over the hemisphere yields the directional hemispherical reflectance,

$$\rho(\theta_i, \phi_i, \lambda) = \int_{2\pi} \rho(\theta_i, \phi_i, \theta_r, \phi_r, \lambda) \cos(\theta_r) d\omega_r. \tag{5}$$

Most materials are isotropic so the azimuthal dependence in equation (5) can be ignored so that,

$$\rho(\theta_i, \phi_i, \lambda) = \rho(\theta, \lambda). \tag{6}$$

The directional emissivity in equation (3) can be computed under Kirchhoff assumptions as,

$$\epsilon(\theta, \lambda) = 1 - \rho(\theta, \lambda). \tag{7}$$

The angular dependence is usually ignored to arrive at the familiar reflectance and emissivity of a material,

$$\epsilon(\lambda) = 1 - \rho(\lambda). \tag{8}$$

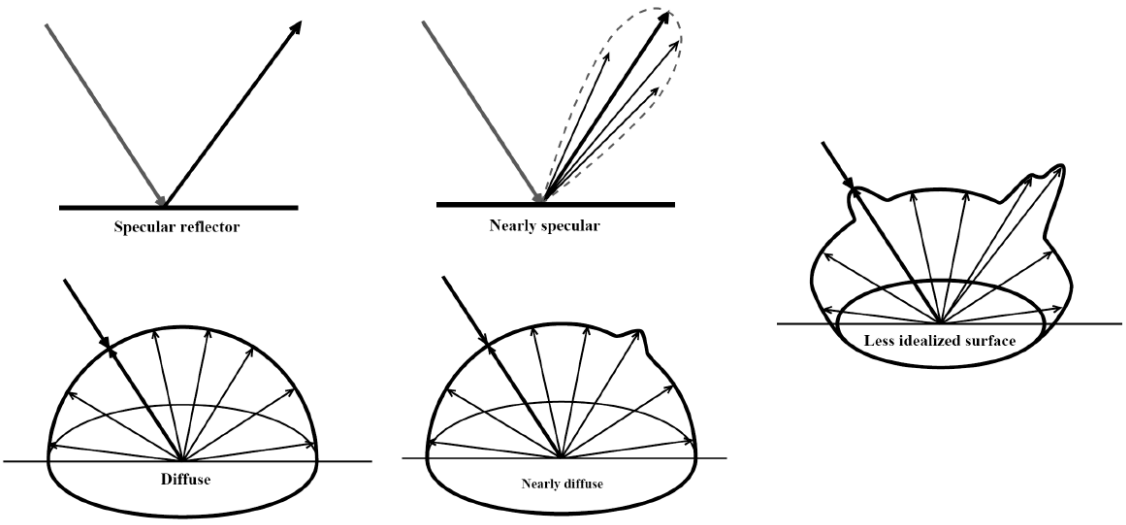

Figure 1. BRDFs for various types of surfaces [3]

Knowledge of the BRDF for the target of interest is very important for the determination of the target's temperature since the BRDF will influence the amount of radiance entering the sensor from which the temperature will be estimated. This is especially important for cavernous targets, and other objects with complex geometries, since the reflected background radiance depends on the BRDF of the target wall and the incident radiance from the surrounding walls and the BRDF for each of these sources.

2.3. BRDF Models

Bidirectional reflectance functions are very difficult to measure directly since spectral measurements must be taken over all incident and reflected angles. In practice semi-empirical models are used to approximate the BRDF based on several measured or estimated parameters. Three such models are briefly introduced here.

2.3.1. Ward Model

The BRDF model described by Ward is a mathematical model designed to approximate a true physical BRDF [4]. The objective was to fit measured reflectance data with a simplistic formula. The Ward formula is based on an isotropic Gaussian distribution of the surface slope. The BRDF of a surface is described as,

$$\rho(\theta_i, \phi_i, \theta_r, \phi_r) = \frac{\rho_d}{\pi} + \rho_s \frac{1}{\sqrt{\cos\theta_i \cos\theta_r}} \frac{\exp\left[-\tan^2\delta/\alpha^2\right]}{4\pi\alpha^2} \qquad \left[sr^{-1}\right], \tag{9}$$

where ρ_d is the diffuse reflectance, ρ_s is the specular reflectance, α is the RMS of the surface slope (similar to surface roughness), and δ is the angle between the surface normal and the vector that bisects the incident and reflected rays. The δ angle is determined by the geometry of the incident and reflected rays. The user is only responsible for providing estimates of ρ_d, ρ_s, and α. A small value of α corresponds to a narrow specular lobe, while a large value corresponds to a wide lobe. The Ward BRDF model is appealing due to its simplicity, however, the model and its input parameters are not based on any physical measurements. Figure (2) illustrates Ward BRDF models for various input parameters.

2.3.2. Priest-Germer Model

The Priest-Germer model is another method of estimating the BRDF of a material [5]. It is capable of producing scalar or polarimetric reflectance functions. The model is based on the assumption that the rough surface of the material is a collection of tiny microfacets. Each microfacet is a specular reflector with a reflectivity given by the Fresnel equations. The normal vectors of the microfacets are assumed to be oriented symetrically about the

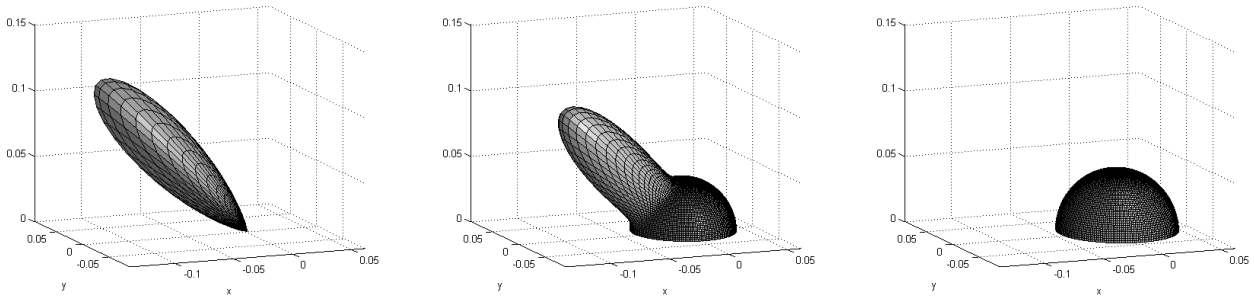

(a) $\rho_d = 0.0$, $\rho_s = 0.035$, $\alpha = 0.15$ (b) $\rho_d = 0.13$, $\rho_s = 0.02$, $\alpha = 0.15$ (c) $\rho_d = 0.13$, $\rho_s = 0.0$, $\alpha = 0.15$

Figure 2. Ward BRDF model with varying specularity and diffuseness

material surface normal according to a Gaussian distribution. Therefore, the value of the BRDF of a particular geometry is the probability that the microfacet is oriented such that an incident ray is reflected into a particular direction. The Priest-Germer BRDF is defined as,

$$\rho_{j,k}(\theta_i, \theta_r, \phi_r - \phi_i) = \frac{1}{2\pi} \frac{1}{4\sigma^2} \frac{1}{\cos^4 \theta} \frac{1}{\cos\theta_r \ \cos\theta_i} \exp\left(\frac{-\tan^2\theta}{2\sigma^2}\right) M_{j,k}(\theta_i, \theta_r, \phi_r - \phi_i) \qquad \left[sr^{-1}\right], \qquad (10)$$

where θ is the angle between the surface normal and the microfacet normal, σ is the surface roughness parameter, and $M_{j,k}(\theta_i, \theta_r, \phi_r - \phi_i)$ is a Mueller matrix whose elements are defined in reference [5].

The model requires knowledge of the complex index of refraction and surface roughness of the material. The complex index of refraction, $n + ik$, is a function of wavelength. The surface roughness, σ, is a parameter that describes the diffuseness of the material. The greater the surface roughness, the more diffuse (less specular) the material is. This model has the advantage that its input parameters are based on physical data about a material.

2.3.3. Beard-Maxwell Model

The Beard-Maxwell model is also based on the microfacet model in which reflection occurs at the first surface but adds a volumetric component in which scattering occurs beneath the surface [1]. The model requires eight input parameters that adjust the scatter from the first surface and from beneath the surface. These parameters are based on actual measured data. This model serves as the basis for the Non-conventional Exploitation Factors Data System (NEFDS). The NEF database contains measured input parameters for several hundred materials. The Beard-Maxwell model along with NEF materials provide a powerful way to generate reflectance models from a few measured parameters for several hundred materials.

2.4. DIRSIG Radiometry

The surface leaving radiance is comprised of reflected and emitted terms. DIRSIG computes the reflected component by sampling the illumination load from the hemisphere and applying the BRDF of the material to each of these incident loading samples. The sampling is driven by the BRDF to insure important directional characteristics, such as specular lobes, are captured [6]. The emissive component is based on the gray body radiance using the surface temperature and the directional emissivity (see equation 3). The directional emissivity is computed from the directional hemispherical reflectance which is numerically integrated from the BRDF (see equation 7).

3. CAVITY MODEL IN DIRSIG

A three-dimensional cavity was modeled in DIRSIG to study the relationship between the number of internal reflections resulting from the cavity geometry and the reflectance characteristics of the internal surfaces on the apparent temperature of the cavity.

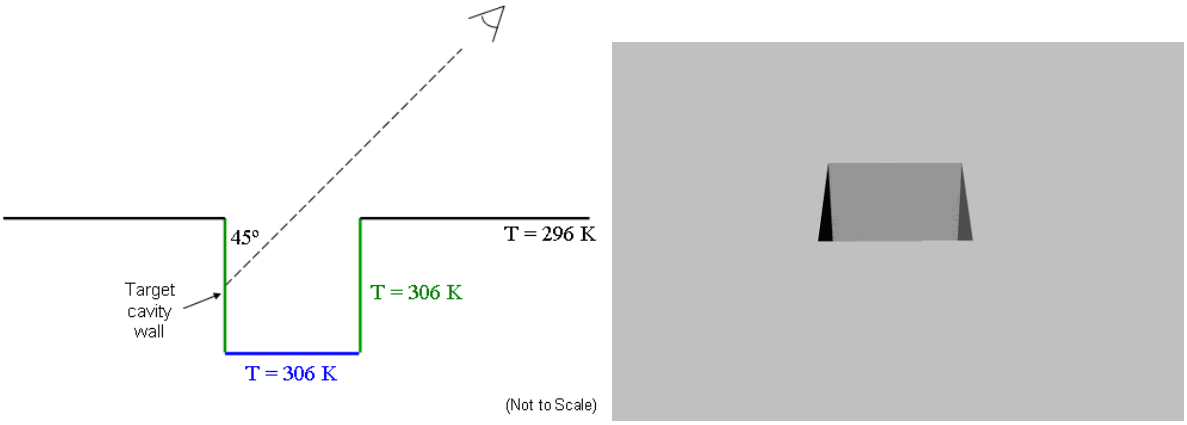

(a) Illustration of cavity layout

(b) CAD rendering of the cavity

Figure 3. Cavity simulation layout

3.1. Description

For this simulation, a hollow square box was placed below a ground plane. The box is open at the top so that an observer can see into the box and the walls are partially exposed to the cold sky. All surfaces of the box are assigned a temperature of 306 K while the ground plane is assigned a temperature of 296 K. The walls of the box, bottom of the box, and ground plane are assigned different material properties. A long wave infrared sensor is positioned above the ground plane and targeted at the far interior wall of the box at an incident angle of 45°. The simulation layout is illustrated in Figure (3).

The radiance incident at the sensor includes contributions from the self-emitted radiance from this cavity wall and radiance reflected from the wall that is incident from the other interior surfaces as well as the sky. The atmosphere was modeled as a spectrally flat 240 K source with a unit transmission and no upwelled path radiance.

The number of internal reflections was controlled by stretching the box downward in fixed increments and also limiting the maximum number of reflections in DIRSIG [2]. The ground plane and bottom surface of the box were assigned spectrally flat emissivities of 1.0 and 0.98, respectively. The emissivity of 0.98 was meant to approximate liquid water (the terminal surface in a cooling tower application). The walls of the box were assigned a Ward BRDF model. This model was chosen due to its relative simplicity and minimal input parameters (see section 2.3.1). The BRDF model requires a diffuse parameter, ρ_d, a specular parameter, ρ_s, and a RMS parameter, α. The diffuse and specular parameters control the magnitude of the diffuse and specular components of the reflectance, respectively. The α parameter controls the width of the specular lobe. Figure (2) illustrates a Ward reflectance model with various parameters.

The DIRSIG simulation of the box was performed with the Ward parameters $\rho_d = 0.02$, $\rho_s = 0.13$, and $\alpha = 0.015$. This case is for a highly specular surface with a tight specular lobe. The directional hemispherical reflectance of this configuration is approximately 0.11 and the emissivity is therefore 0.89 according to Kirchhoff's law. The radiance reaching the sensor was recorded as a function of the number of internal reflections used in the simulation. As noted previously, the number of reflections is controlled by stretching the box downward in increments equal to the original length of the box, subsequently moving the terminal surface lower, and by limiting the maximum bounce count in DIRSIG. The integrated radiance was converted to an apparent temperature for subsequent analysis.

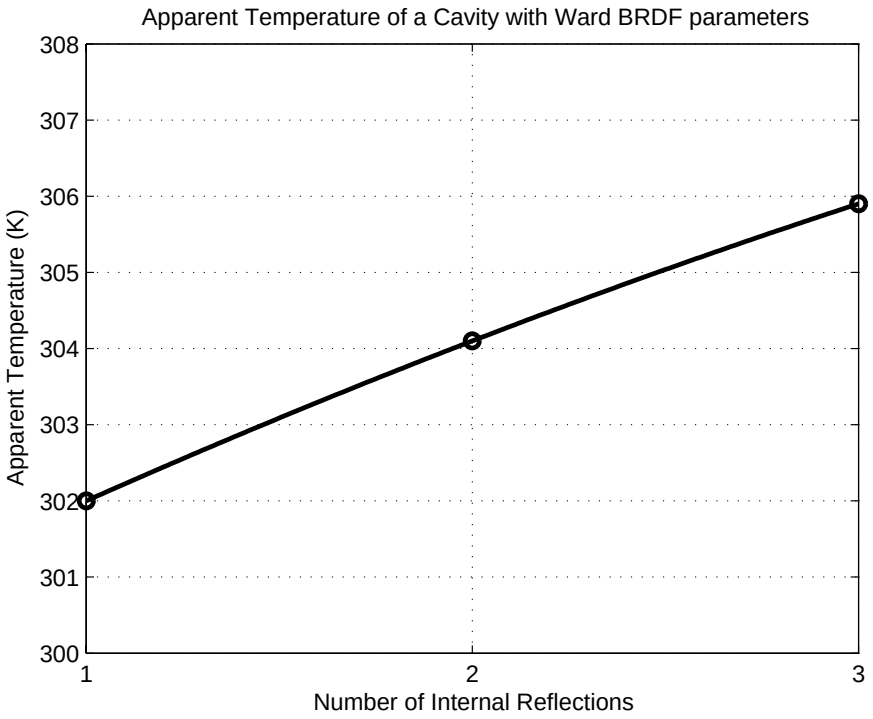

Figure 4. Apparent temperature dependence on the number of internal reflections using a Ward BRDF with parameters: $\rho_d = 0.02$, $\rho_s = 0.13$, $\alpha = 0.015$. The actual temperature of the cavity was 306 K.

3.2. Results

The DIRSIG runs were performed for one, two, and three internal reflections. The number of trials was limited by the relatively long run times associated with the ray-tracing internal to DIRSIG. Figure (4) shows the results of the simulations.

Theoretically despite the fact that the observed surface has an emissivity less than unity, the apparent temperature of the cavity should increase and approach the actual assigned temperature as the number of reflections increases since the cavity should act more like a blackbody. The apparent temperature of the target recorded at the sensor increased as more internal reflections are included in the simulation. The apparent temperature arrived at the actual blackbody temperature of 306 K for the cavity after three reflections. The results from Figure (4) appear to agree with theory. Since the walls of the cavity have an emissivity of about 0.89, their reflectance is 0.11 via Kirchoff's law (see equation 8). The radiance incident on the sensor is the sum of the self-emitted radiances of all the surfaces after being reflected by subsequent internal components. For example, for just one reflection the radiance reaching the sensor is,

$$L = \epsilon L_{BB} + \rho L_{bkgd} \qquad \left[\frac{W}{m^2\ sr}\right]. \tag{11}$$

Note that the wavelength dependence has been omitted for clarity. The first term is the self-emitted radiance from the first surface of the cavity that the sensor sees directly. The second term is the composite reflected background radiance. For the highly specular Ward BRDF used in this simulation, the background radiances consist exclusively of the other walls of the cavity. If a diffuse BRDF were used, the background radiances would consist of the other walls and the sky. As the number of reflections inceases, the background radiance values increase causing the apparent temperature at the sensor to increase until the blackbody temperature of the cavity is reached. For the diffuse case, the apparent temperature would approach the blackbody temperature more slowly.

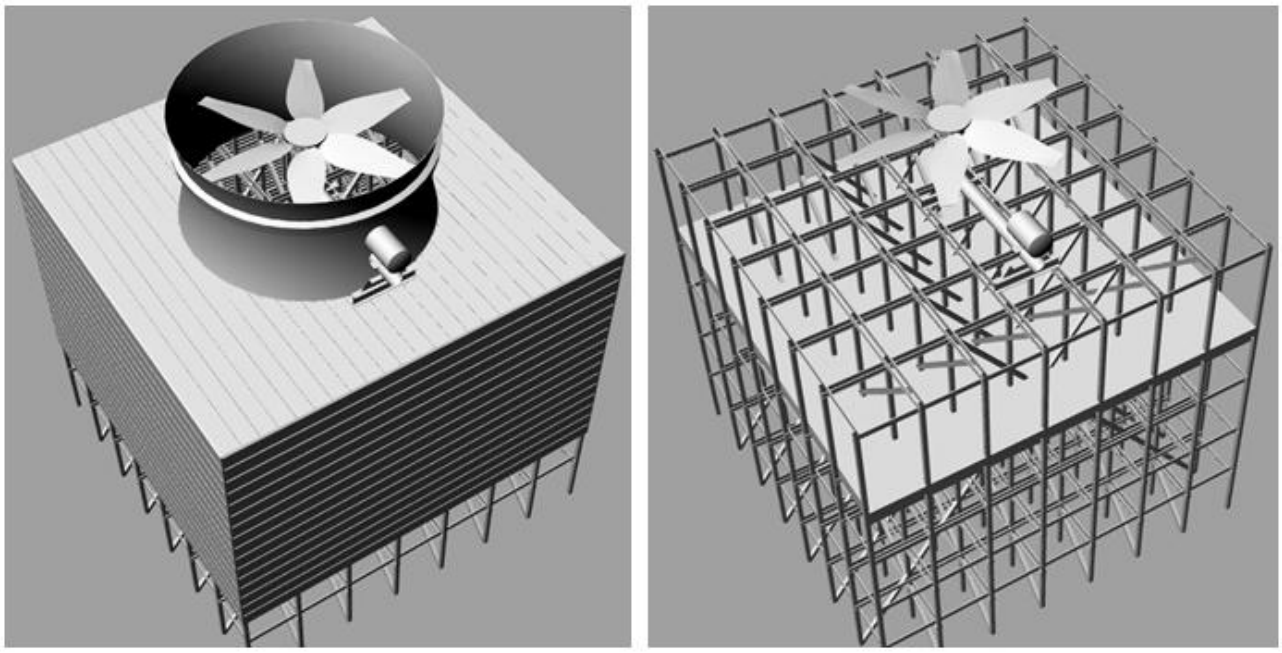

Figure 5. CAD drawing of a counter-flow cooling tower exterior view (left) and interior view (right).

4. MDCT MODEL IN DIRSIG

The cavity model was then extended to a detailed model of a mechanical draft cooling tower (MDCT). Determination of an accurate temperature of a MDCT is important for certain surveillance applications.

4.1. Description

The DIRSIG rendering of a MDCT was generated by assigning basic thermal properties to a geometric model of a tower. The geometrically detailed three-dimensional CAD drawing was intended to mimic a counter-flow tower similar to the H-area units at the Savannah River Site (SRS). The geometry of the drawing was based on measurements taken at SRS and on schematics made available by the manufacturer [7]. A high fidelity geometric model is necessary to reproduce the geometry for multiple reflections within the cooling tower. The detailed CAD model is shown in Figure (5). For this initial simulation, each facet of the model was assigned a temperature of 306 K and diffuse emissivity of 0.75. Future work will measure real emissivities for these materials. A broadband 8 - 14 μm sensor was positioned 25° from zenith at a distance of 120 m from the tower throat. The environmental parameters in the simulation were set to approximate typical summer conditions at the Savannah River Site. The output of the DIRSIG simulation is an integrated radiance image of the tower in the longwave infrared. As before, the radiance values were converted to apparent temperature.

4.2. Results

The DIRSIG output is a radiance image of the tower at the entrance aperture of the sensor. Bright pixels indicate higher radiances while dark pixels indicate lower radiance values. The DIRSIG rendering is shown in Figure (6).

A quick look at the DIRSIG image indicates that the phenomenology that is produced is as expected. The brightest pixels, representing the highest temperatures, are deep within the tower. The exterior of the tower appears cooler than the interior because it partially reflects the colder sky. The ground plane was assigned a temperature of 288 K and makes up the darkest pixels in the image.

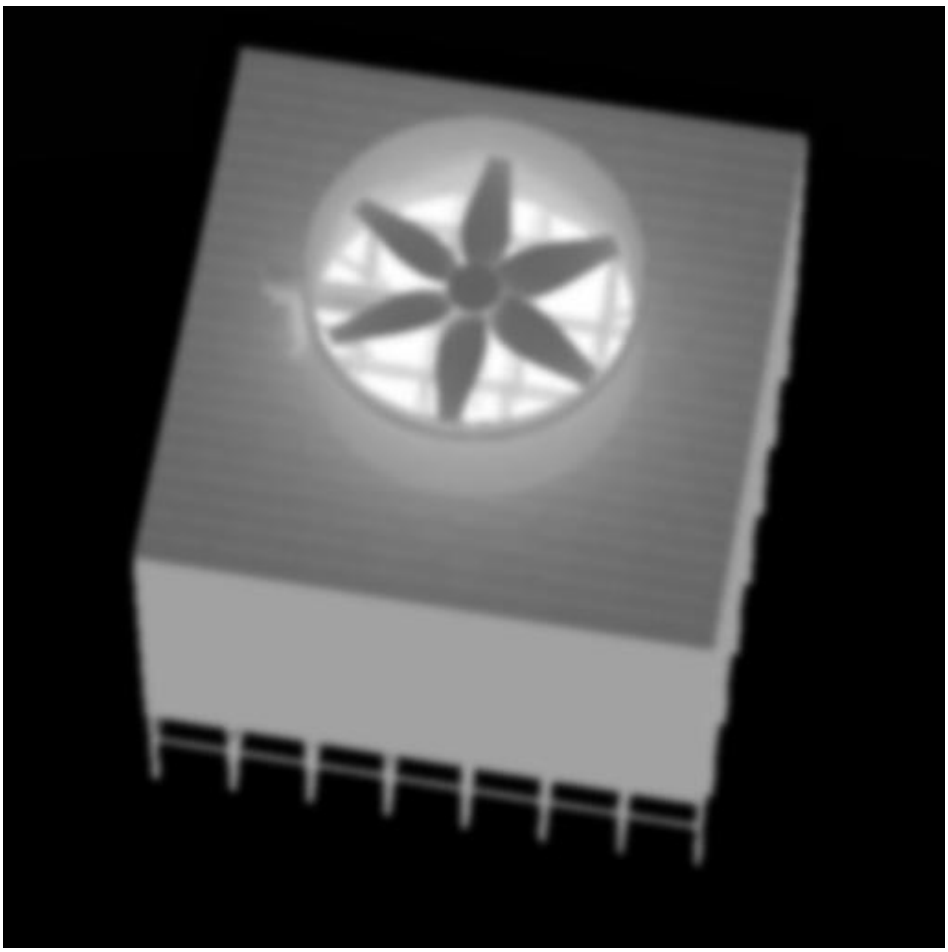

Figure 6. DIRSIG rendering of a MDCT

During preliminary analysis, a comparison was made between the DIRSIG image and an actual infrared image obtained of a counter-flow tower at SRS. The SRS image was obtained from a helicopter based infrared imaging system. The tower in this image was operating in the "water running, fans off" mode meaning that the tower was being used to passively cool the water. A radiance profile through the tower throat was taken and converted to apparent temperature. A similar profile was taken on the SRS image. The profile locations in the DIRSIG and the SRS images are shown in Figure (7) and the brightness temperature across these profiles are shown in Figure (8).

Figure (8) demonstrates that the temperature profile for the DIRSIG image matches the general shape of the temperature profile for the SRS image. The highest values in the plots are pixels located deep within the tower. The central depression indicates the fan hub while the low temperature values at the left and right extremes of the plots indicate the tower decking. The apparent temperatures at these points are lower than the interior of the tower due to the reflected sky temperature. The temperature contrast in the DIRSIG plot is roughly double that of the SRS plot. This difference is attributed to the fact that the actual material parameters that make up the SRS tower have not been measured at this time and have been approximated for these simulations.

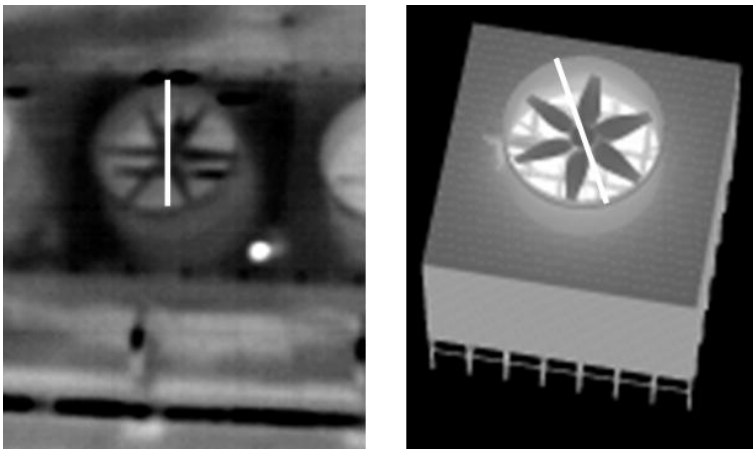

Figure 7. SRS image (left) and DIRSIG image (right). Profiles indicated by solid white line.

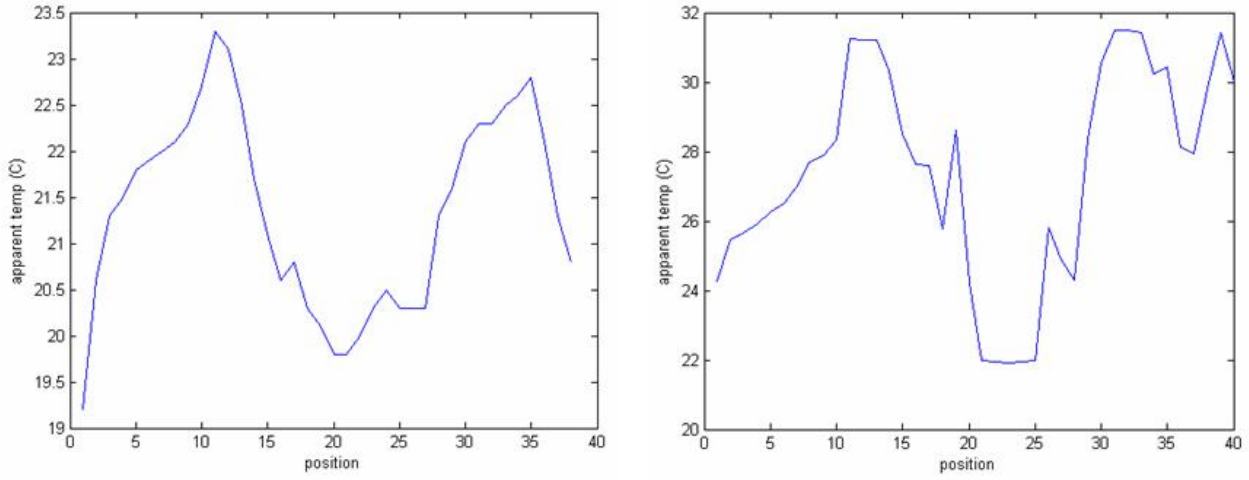

Figure 8. Apparent temperature profiles across the tower throat for the SRS image (left) and DIRSIG image (right).

5. CONCLUSIONS

Derivation of the absolute temperature of a cavity represents a complex radiometric inversion problem. The apparent temperature is dependent on the material properties of the interior surfaces of the cavity as well as the internal geometry of the cavity. The results of the cavity simulation in DIRSIG revealed that the apparent temperature of the cavity increased and approached the actual temperature of the cavity as the number of internal reflections increased. The apparent temperature reached the actual temperature after three reflections. This result agrees with expectations since a cavity should behave as a blackbody as the number of internal reflections increases. The results of the MDCT DIRSIG simulation show that a detailed geometric model along with basic thermal properties can produce a good qualitative approximation of the apparent temperatures of a mechanical draft cooling tower. The DIRSIG simulations revealed that the absolute temperature of a cavernous object can be determined from remotely sensed thermal imagery provided the complex radiometric interactions are understood and accounted for.

6. FUTURE WORK

Near-term work will focus on re-running the simple cavity in DIRSIG with various Ward BRDF parameters. This will allow us to study the effects of various BRDF parameters on the apparent temperature of the cavity. In addition, the cavity simulation will be performed with other BRDF models, such as the Priest-Germer model which is already implemented in DIRSIG. The long-term goal is to incorporate the NEFDS implementation of the Beard-Maxwell BRDF model in DIRSIG. This model along with the NEF material database will allow DIRSIG users to assign NEF materials to object facets in the DIRSIG environment. The full MDCT DIRSIG model discussed in this report will be updated to include NEF materials in order to increase the radiometric accuracy of the model.

ACKNOWLEDGMENTS

The authors would like to extend a special thanks to the DIRS laboratory at the Center for Imaging Science at RIT, in particular to Niek Sanders for his DIRSIG support and to the Savannah River National Laboratory for their sponsorship under contract DE-AC09-96SR18500.

REFERENCES

1. "Nonconventional Exploitation Factors (NEF) Modeling," Tech. Rep. v9.5, April 2005.
2. Digital Imaging and Remote Sensing Laboratory, Rochester, NY, *The DIRSIG User's Manual*, February 2006.
3. J. R. Schott, *Remote Sensing: The Image Chain Approach*, Oxford University Press, New York, NY, 1997.
4. G. J. Ward, "Measuring and Modeling Anisotropic Reflection," in *Computer Graphics*, pp. 265–272, July 1992.
5. R. G. Priest and T. A. Germer, "Polarimetric BRDF in the Microfacet Model: Theory and Measurements," in *Proceedings of the 2000 Meeting of the Military Sensing Symposia Specialty Group on Passive Sensors*, **1**, pp. 169–181, 2002.
6. A. Goodenough, R. Raqueño, M. Bellandi, S. Brown, and J. Schott, "A Flexible Hyperspectral Simulation Tool for Complex Littoral Environments," in *Photonics for Port and Harbor Security II*, SPIE Vol. 6204, 2006.
7. SPX Cooling Technologies, Inc., Overland Park, KS, *http://spxcooling.com/en/*.